Article

Not peer-reviewed version

Cascadable First-Order and Second-Order Inverse Filters Based On Second-Generation Voltage Conveyors

Natchanai Roongmuanpha , Nutcha Likhitkitwoerakul , Tattaya Pukkalanun , Mohammad Faseehuddin , Worapong Tangsrirat *

Posted Date: 14 January 2025

doi: 10.20944/preprints202501.0957.v1

Keywords: second-generation voltage conveyor (VCII); inverse filter; first-order filter; second-order filter; voltage-mode circuit; current-mode circuit

Article

Cascadable First-Order and Second-Order Inverse Filters Based on Second-Generation Voltage Conveyors

Natchanai Roongmuanpha [1], Nutcha Likhitkitwoerakul [2], Tattaya Pukkalanun [1], Mohammad Faseehuddin [3] and Worapong Tangsrirat [1,*]

[1] School of Engineering, King Mongkut's Institute of Technology Ladkrabang (KMITL), Bangkok 10520, Thailand; natchanai.ro@kmitl.ac.th, tattaya.pu@kmitl.ac.th

[2] Ministry of Natural Resources and Environment, Phaya Thai, Bangkok 10400, Thailand; nutcha.likhitkit@gmail.com

[3] Department of Electronics and Communication Engineering, Thapar Institute of Engineering and Technology, Patiala, Punjab 147004, India; faseehuddin03@gmail.com

* Correspondence: worapong.ta@kmitl.ac.th

Abstract: This study introduces four novel configurations of first-order and second-order multifunction inverse filters in both voltage-mode (VM) and current-mode (CM) using second-generation voltage conveyors (VCIIs). The first-order VM and CM inverse filters utilize only three passive components together with one VCII for VM and two VCIIs for CM realizations, which can provide lowpass (LP) and highpass (HP) inverse filter responses through appropriate impedance selections. The latter, second-order VM and CM multifunction inverse filters, can be constructed using the corresponding first-order inverse filters as their core circuits. These filters offer all the basic inverse filter functions, including LP, bandpass (BP), and HP inverse responses with all gains obtained from the same design. All the CM inverse filter realizations possess low-input and high-output impedances, enabling them to be fully cascaded in CM operation. For the VM filter realizations, they exhibit low-output impedances, which directly connect to the next stage without any buffer requirement. No component matching requirements are necessary for all filter responses. The non-ideal effects of the VCII on the performance of the proposed inverse filters are thoroughly examined, taking into account undesirable aspects such as tracking errors and parasitic impedances. To prove the feasibility of the designs, PSPICE program performed several simulations, utilizing model parameters of 0.18-μm CMOS technology. In addition, some testing experiments are conducted using the commercially available IC-type AD844s for evaluating the practical performance of the designed inverse filters

Keywords: second-generation voltage conveyor (VCII); inverse filter; first-order filter; second-order filter; voltage-mode circuit; current-mode circuit

1. Introduction

In control and instrumentation, and speech applications, inverse filters are crucial circuit components used to correct distorted output signals resulting from linear or nonlinear transformations caused by signal processors or transmission systems. This filter has a frequency response that is inversely proportional to the frequency response of the system, leading to distortion. The design of inverse filters is also necessary in several communication applications, such as monitoring the relative cleanness of a signal and de-emphasizing FM systems. In control systems, it is necessary to employ inverse lowpass, highpass, and bandpass filter functions for the implementation of proportional-integral (PI), proportional-derivative (PD), and proportional-integral-derivative (PID) controllers. For these reasons, the literature in [1-31] explicitly discusses the design and implementation of inverse filters utilizing different modern active components. The

Preprints.org (www.preprints.org) | NOT PEER-REVIEWED | Posted: 14 January 2025 doi:10.20944/preprints202501.0957.v1

previous studies aim to operate in various modes such as voltage mode (VM) [1,6,8-11,13-15,17-31], current mode (CM) [2-5,7,12,14,15,17,30], and trans-admittance mode (TAM) [16]. In addition, the works of [5-7,23,29,31] are developed specifically as first-order inverse filters, whereas the works referenced as [1-4,8-24,26-30] deal with second-order inverse filters.

In [1], a comprehensive approach utilizing nullors as fundamental components was introduced to derive the inverse transfer function for linear dynamic systems and the inverse transfer characteristic for non-linear resistive circuits. An example of a Sallen-Key highpass filter and the inverse of a half-wave rectifier has also been used to illustrate this approach. The previous study described in [2] provided a procedure for transforming a VM op-amp-based RC filter into CM, four-terminal floating nullor (FTFN)-based inverse filter. The realization approach employs a network representation that utilizes nullors and RC:CR dual transformation. The work in [3] demonstrates a general method for deriving FTFN-based CM inverse filters from well-known VM filters, as well as generating a CM inverse filter from the Friend-Delyannis biquad. Since FTFN is not available commercially, one can realize it using two second-generation current conveyors (CCIIs) or two current feedback operational amplifiers (CFOAs). A number of CM inverse filter implementations using a single FTFN has been described in [4], where the simulation results reported in this study were obtained by synthesizing the FTFN using two CCIIs. Numerous additional inverse filters were given in [5-8,16,20-25]. Each configuration provides a single inverse filter function. Multifunction second-order VM and TAM inverse filter realizations employing more than two active components are suggested in [8-11,14-17,19, 26,27,29]. Some of them also necessitate a significant number of passive components for their realizations, at least seven passive components [17,20[21,24,25,29,30]. In [12], it is observed that the output current of the CM inverse filter is sensed through the passive components, requiring an additional buffer stage to connect to the next stage. The output voltage terminals of the second-order VM inverse filter designs in [13,14,18-21,23,24,28] do not explicitly have a low impedance level. Thus, these filters are not appropriate for cascadable connections.

This study emphasizes the use of second-generation voltage conveyors (VCIIs) as active components in designing multifunction inverse filters. Four configurations implementing first-order and second-order inverse filters in both VM and CM are presented. The suggested first-order VM inverse filter employs only one VCII and three passive components to realize both inverse LP and HP filter functions by appropriately selecting the external impedance type. With its very low output impedance, it is suitable for cascading in VM operation. By cascading the suggested first-order VM inverse filter, the second-order VM inverse filter with all the generic inverse filter realizations, i.e., LP, BP and HP, can be obtained. The third proposed circuit features a first-order CM configuration with two VCIIs and three passive elements. On the other hand, the fourth configuration is the second-order CM type that provides inverse LP, HP, and AP filter responses within the same circuit design. Both of the proposed CM inverse filters exhibit a low-input impedance and a high-output impedance, which permits full cascadability. All of the proposed circuits possess the characteristic of orthogonal control of their pole frequency and minimum gain, and do not require any criteria for component matching. The theoretical predictions are confirmed by PSPICE simulation results using TSMC 0.18-μm CMOS model parameters. Furthermore, the laboratory testing involved the utilization of commercially available IC-type AD844 CFOAs for measurement purposes. Table 1 provides a comprehensive comparison between previously available inverse filters and the proposed circuits in terms of operation mode, filter order, available response, active and passive component count, technology required, supply voltage levels, and power dissipation.

Table 1. Comparison of the previously available inverse filters and the proposed circuits.

Ref./ Year	Mode of operation	Order of filter	Type of filter	No. of active components	No. of passive components	Technology	Supply voltages (V)	Power dissipation (mW)
[1]/1997	VM	2nd	IHP	1 OA	4R + 2C	N/A	N/A	N/A
[2]/1999	CM	2nd	ILP	1 FTFN	5R + 2C	AD704, 2N2222, 2N2907	N/A	N/A

Preprints.org (www.preprints.org) | NOT PEER-REVIEWED | Posted: 14 January 2025 doi:10.20944/preprints202501.0957.v1

[3]/1999	CM	2nd	IAP	1 FTFN	4R + 2C	N/A	N/A	N/A
[4]/2000	CM	2nd	ILP, IBP, IHP, IBS, IAP	1 FTFN	ILP: 3R + 2C, IBP, IHP: 2R+3C, IBS, IAP: 4R+2C	AD844	N/A	N/A
[5]/2005	CM	1st	IAP	1 FTFN	3R + 1C	AD844	N/A	N/A
[6]/2006	VM	1st	IAP	1 CCII	2R + 1C	AD844	N/A	N/A
[7]/2008	CM	1st	IAP	1 CDTA	1R + 1C	NR100N, PR100N	±3	N/A
[8]/2009	VM	2nd	ILP, IBP, IHP, IBS	3 CFOA	4R + 2C	AD844	±12	N/A
[9]/2011	VM	2nd	ILP, IBP, IHP	3 CFOA	ILP: 3R + 2C, IBP: 2R + 4C, IHP: 3R + 3C	AD844	±12	N/A
[10]/2011	VM	2nd	ILP, IBP, IHP, IBS	3 CFOA	ILP: 3R + 2C, IBP: 4R+ 2C, IHP, IBS: 5R+2C	AD844	±12	N/A
[11]/2012	VM	2nd	ILP, IBP, IHP	3 MCFOA	ILP: 3R + 2C, IBP, IHP: 3R+3C	TSMC 0.25 μm	±1.25, +0.8	N/A
[12]/2013	CM	2nd	ILP, IBP, IHP	2 CDBA	ILP: 4R + 2C, IBP: 3R + 3C, IHP: 2R + 4C	AD844	±12	N/A
[13]/2013	VM	2nd	ILP, IBP, IHP, IBS, IAP	2 CDBA	ILP: 4R + 2C, IBP: 3R + 3C, IHP: 2R + 4C, IBS, IAP: 4R+4C	AD844	±10	N/A
[14]/2014	VM, CM	2nd	ILP, IBP, IHP	ILP, IBP: 6 OTA, IHP: 5 OTA	2C	MOSIS 0.5 μm	±1.8	1.33~2.0
[15]/2015	VM	2nd	ILP, IBP, IHP, IBS	2 CFOA	ILP, IBP, IHP: 4R+2C, IBS: 6R + 2C	AD844	N/A	N/A
	CM	2nd	ILP	3 CFOA	3R + 2C			
[16]/2015	TAM	2nd	IHP	3 CDTA	2R + 2C	MOSIS 0.35 μm	±3.5	N/A
[17]/2018	VM	2nd	ILP, IBP, IHP	ILP, IBP: 6 CCII, IHP: 5 CCII	ILP, IBP: 6R+2C, IHP: 5R+2C	MOSIS 0.5 μm	±1.85	7.01~10.2
	CM	2nd	IAP	3(4) CCII	IAP: 3(4)R+2C			
[18]/2018	VM	2nd	ILP, IBP, IHP	2 OTRA	ILP, IBP: 4R+2C, IHP: 3R+3C	TSMC 0.18 μm	N/A	N/A
[19]/2018	VM	2nd	ILP, IBP, IHP, IBS	ILP, IBP, IBS: 3 VDTA, IHP: 2 VDTA Unified filter: 4 VDTA, 2 SW	2C 3C	TSMC 0.18 μm	±0.9	N/A
[20]/2019	VM	2nd	IBS, IAP	2 OTRA	4(6)R + 3(4)C	TSMC 0.18 μm	±0.9, -0.3	N/A

[21]/2019	VM	2nd	IBS, IAP	2 CDBA, 1 SW	5R + 2C	TSMC 0.18 μm	±2.5	N/A
[22]/2019	VM	2nd	IBS, IAP	2 CDBA	4R + 2C	TSMC 0.18 μm	±2.5	N/A
[23]/2019	VM	1st	ILP, IHP	1 OA	ILP: 1(2)R + 1C, IHP: 1(2)R + 1(2)C	VCVS macro model	N/A	N/A
		2nd	IBP	1 OA	2R + 2C			
[24]/2019	VM	2nd	IBS	1 OTRA, 3 SW	5R + 5C	CMOS 0.18 μm	±1.5, -0.5	1.46
[25]/2020	VM	6th	IBP	2 CDBA	9R + 9C	TSMC 0.18 μm	±0.6	0.918
[26]/2021	VM	2nd	ILP, IBP, IHP, IBS	4 VDTA, 3 SW	2C	TSMC 0.18 μm	±0.9	2.16
[27]/2021	VM	2nd	ILP, IBP, IHP, IBS	ILP, IBP, IHP: 4 OTA, IBS: 5 OTA	2C	TSMC 0.18 μm	±0.9, -0.6~-0.78	N/A
[28]/2021	VM	2nd	ILP, IBP, IHP, IBS	1 CDBA	ILP: 3R + 2C, IBP, IBS: 2R + 2C, IHP: 2R + 3C	TSMC 0.35 μm	±2.5	N/A
[29]/2021	VM	1st	ILP, IHP	2 VCII	4R + 1C	TSMC 0.18 μm	±0.9	0.6
		2nd	IBP	3 VCII	6R + 2C			
[30]/2022	VM	2nd	IBP	2 VCII	5R + 2C	TSMC 0.18 μm	±0.9	N/A
	CM	2nd	ILP, IBP, IHP, IBS		2R + 2C			
[31]/2024	VM	1st	ILP, IHP	2 CFOA	3R + 2C	AD844	N/A	N/A
This work	VM (Fig. 2)	1st	ILP, IHP	1 VCII	ILP: 1R + 2C, IHP: 2R + 1C	TSMC 0.18 μm	±0.75	0.255
		2nd	ILP, IBP, IHP	2 VCII	ILP: 2R + 4C, IBP: 3R + 3C, IHP: 4R + 2C			0.511
	CM (Fig. 3)	1st	ILP, IHP	2 VCII	ILP: 1R + 2C, IHP: 2R + 1C			0.511
		2nd	ILP, IBP, IHP	3 VCII	ILP: 4R + 2C, IBP: 3R + 3C, IHP: 4R + 2C			0.766

2. Second-Generation Voltage Conveyor (VCII)

The proposed designs are based on the use of the VCII as an active element. The VCII is symbolically represented in Figure 1, which also provides the following description of its terminal relationship:

$$v_y = 0, \quad i_x = \pm\beta i_y, \quad \text{and} \quad v_z = \alpha v_x, \tag{1}$$

where β is the current gain between the y and x terminals, and α is the voltage gain between the x and z terminals. In ideal case, the gain values β and α are both equal to unity. The "+" and "–" signs in Equation (1) indicate the positive VCII (VCII+) and negative VCII (VCII-), respectively. Equation (1) also reveals that the VCII has a low-input impedance y terminal, a high-output impedance x terminal, and a low-output impedance z terminal.

Preprints.org (www.preprints.org) | NOT PEER-REVIEWED | Posted: 14 January 2025 doi:10.20944/preprints202501.0957.v1

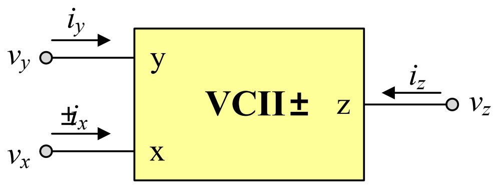

Figure 1. Electrical symbol of the VCII.

3. Proposed Cascadable Voltage-Mode Inverse Filters

Using the VCII in Figure 1 as an active component, the implementations of the first-order and second-order VM inverse filters are demonstrated in Figure 2.

3.1. First-Order VM Inverse Filter Realization

Figure 2a depicts the realization of the first-order VM inverse filter. The circuit requires one VCII-, one resistor (R_1), one capacitor (C_1), and one impedance (Z_A). It is worth noting that the output voltage terminal of the circuit is directly obtained from the z terminal of VCII-. This configuration offers the benefit of a cascadable terminal with a low output impedance. A straightforward circuit analysis assuming ideal VCII yields the following inverse filter transfer function:

$$G_{v1}(s) = \frac{V_{out1}(s)}{V_{in}(s)} = \frac{sR_1C_1 + 1}{sC_1Z_A} \tag{2}$$

Equation (2) clearly indicates that, by appropriately configuring the impedance Z_A, the first-order ILP and IHP filter responses could be realized in a single configuration, as demonstrated in Table 2. As can also be seen from the table, the gain (G_0) values of ILP and IHP filters can be tuned independently through C_A and R_A, respectively. An additional advantage of this realization is that no element-matching realizability conditions are necessary.

3.2. Second-Order VM Inverse Filter Realization

Figure 2b illustrates the proposed realization of the second-order VM inverse filter, which is constructed using the cascade connection of the first-order VM inverse filter in Figure 2a. This topology still exhibits a low output impedance, making it appropriate for cascading in VM operation. The voltage transfer function of the circuit is given by:

$$G_{v2}(s) = \frac{v_{out2}}{v_{in}} = \frac{N(s)}{s^2C_1C_2Z_AZ_B} \quad , \tag{3}$$

where
$$N(s) = s^2R_1R_2C_1C_2 + s\left(R_1C_1 + R_2C_2\right) + 1 \quad . \tag{4}$$

Similarly, the suitable impedance choices for Z_A and Z_B as specified in Table 3 would lead to the required second-order ILP, IHP, and IBP filter responses.

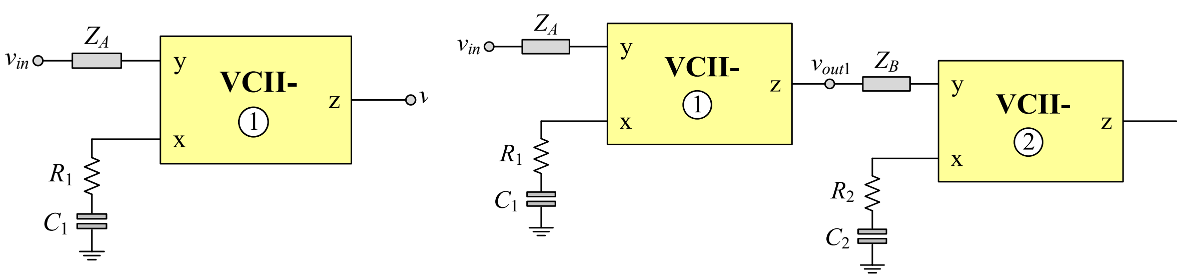

Preprints.org (www.preprints.org) | NOT PEER-REVIEWED | Posted: 14 January 2025 doi:10.20944/preprints202501.0957.v1

(**a**) (**b**)

Figure 2. Proposed VCII-based VM inverse filters. (**a**) 1st-order filter; (**b**) 2nd-order filter.

Table 2. Selection of impedance Z_A for the first-order VM inverse filter in Figure 2a.

Filter type	Z_A	Transfer function, $G_{v1}(s)=\frac{V_{out1}(s)}{V_{in}(s)}$	Minimum gain (G_0)	Cut-off frequency (ω_0)
ILP	$\frac{1}{sC_A}$	$G_0\left(sR_1C_1+1\right)$	$\frac{C_A}{C_1}$	$\frac{1}{R_1C_1}$
IHP	R_A	$G_0\left(\frac{sR_1C_1+1}{sR_1C_1}\right)$	$\frac{R_1}{R_A}$	$\frac{1}{R_1C_1}$

Table 3. Selection of impedances Z_A and Z_B for the second-order VM inverse filter in Figure 2b.

Filter type	Z_A	Z_B	Transfer function, $G_{v2}(s)=\frac{V_{out2}(s)}{V_{in}(s)}$	Minimum gain (G_0)	Cut-off frequency (ω_0)	Quality factor (Q)
ILP	$\frac{1}{sC_A}$	$\frac{1}{sC_B}$	$G_0N(s)$	$\frac{C_AC_B}{C_1C_2}$		
IHP	R_A	R_B	$G_0\left[\frac{N(s)}{s^2R_1R_2C_1C_2}\right]$	$\frac{R_1R_2}{R_AR_B}$	$\frac{1}{\sqrt{R_1R_2C_1C_2}}$	$\frac{\sqrt{R_1R_2C_1C_2}}{R_1C_1+R_2C_2}$
IBP	$\frac{1}{sC_A}$	R_B	$G_0\left[\frac{N(s)}{s\left(R_1C_1+R_2C_2\right)}\right]$	$\left(\frac{R_1}{C_2}+\frac{R_2}{C_1}\right)\left(\frac{C_A}{R_B}\right)$		

4. Proposed Cascadable Current-Mode Inverse Filters

4.1. First-Order CM Inverse Filter Realization

By slightly modifying the configuration depicted in Figure 2a, the circuit can perform a CM inverse filter as shown in Figure 3a. It consists of a primary circuit from Figure 2a and an additional VCII- #2. Due to its low input impedance and high output impedance, the scheme supports cascading inputs and outputs for CM operation. By selecting of the appropriate impedance Z_A, the proposed circuit in Figure 3a generates the following filter-order inverse frequency response for CM at the terminal i_{out1}, which possess the critical characteristics detailed in Table 4.

$$G_{i1}(s)=\frac{I_{out1}(s)}{I_{in}(s)}=\frac{sR_1C_1+1}{sC_1Z_A}\quad. \tag{5}$$

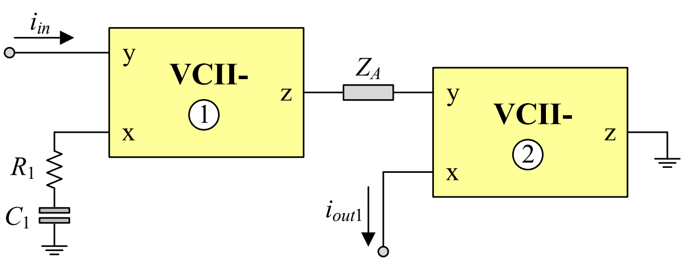

(a)

Preprints.org (www.preprints.org) | NOT PEER-REVIEWED | Posted: 14 January 2025 doi:10.20944/preprints202501.0957.v1

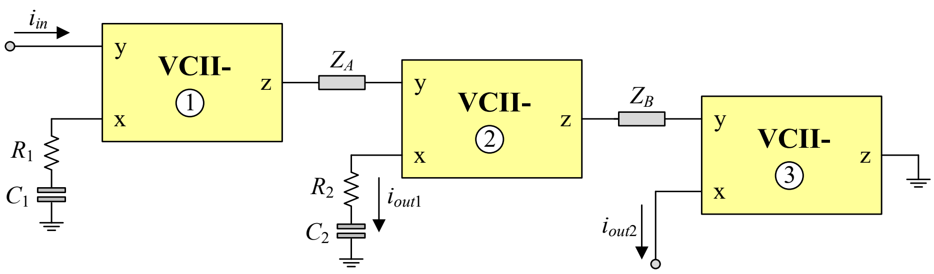

(b)

Figure 3. Proposed VCII-based CM inverse filters. (**a**) 1st-order filter; (**b**) 2nd-order filter.

Table 4. Selection of impedance Z_A for the first-order CM inverse filter in Figure 3a.

Filter type	Z_A	Transfer function, $G_{i1}(s)=\frac{I_{out1}(s)}{I_{in}(s)}$	Minimum gain (G_0)	Cut-off frequency (ω_0)
ILP	$\frac{1}{sC_A}$	$G_0\left(sR_1C_1+1\right)$	$\frac{C_A}{C_1}$	$\frac{1}{R_1C_1}$
IHP	R_A	$G_0\left(\frac{sR_1C_1+1}{sR_1C_1}\right)$	$\frac{R_1}{R_A}$	$\frac{1}{R_1C_1}$

4.2. Second-Order CM Inverse Filter Realization

The construction of the second-order CM inverse filter in Figure 3b involves cascading the first-order section of VCII- #2, R_2, C_2, and Z_B from Figure 3a. The resulting circuit realizes the following CM transfer function at the current output terminal, i_{out2}.

$$G_{i2}(s)=\frac{i_{out2}}{i_{in}}=\frac{N(s)}{s^2C_1C_2Z_AZ_B}\ . \tag{6}$$

By choosing the impedances Z_A and Z_B as shown in Table 5, one can then realize three different second-order CM inverse filter functions.

Table 5. Selection of impedances Z_A and Z_B for the second-order CM inverse filter in Figure 3b.

Filter type	Z_A	Z_B	Transfer function, $G_{v2}(s)=\frac{V_{out2}(s)}{V_{in}(s)}$	Minimum gain (G_0)	Cut-off frequency (ω_0)	Quality factor (Q)
ILP	$\frac{1}{sC_A}$	$\frac{1}{sC_B}$	$G_0N(s)$	$\frac{C_AC_B}{C_1C_2}$		
IHP	R_A	R_B	$G_0\left[\frac{N(s)}{s^2R_1R_2C_1C_2}\right]$	$\frac{R_1R_2}{R_AR_B}$	$\frac{1}{\sqrt{R_1R_2C_1C_2}}$	$\frac{\sqrt{R_1R_2C_1C_2}}{R_1C_1+R_2C_2}$
IBP	$\frac{1}{sC_A}$	R_B	$G_0\left[\frac{N(s)}{s\left(R_1C_1+R_2C_2\right)}\right]$	$\left(\frac{R_1}{C_2}+\frac{R_2}{C_1}\right)\left(\frac{C_A}{R_B}\right)$		

5. Tracking Error Analysis

In non-ideal operation, current and voltage transfer errors may cause deviations in the actual values of the proposed filters. To evaluate the effect of the VCII tracking errors on the circuit performance, the gain values β and α of the k-th VCII-, where k = 1, 2, and 3, are defined as β_k and α_k, respectively. We also denote that $\beta_k = (1 - \varepsilon_i)$ and $\alpha_k = (1 - \varepsilon_v)$, where ε_i ($|\varepsilon_i| \ll 1$) and ε_v ($|\varepsilon_v| \ll 1$) are the current and voltage tracking errors, respectively.

Preprints.org (www.preprints.org) | NOT PEER-REVIEWED | Posted: 14 January 2025 doi:10.20944/preprints202501.0957.v1

Consequently, we perform non-ideal analyses of the proposed circuits in Figure 2 and report their non-ideal parameters in Tables 6 and 7. Following a similar manner, we also analyze the circuits depicted in Figure 3 for non-ideal transfer gains and present the non-ideal parameters in Tables 8 and 9.

From Tables 6-9, it is obvious that the non-ideal values of ω_0 and Q are not influenced by the current and voltage tracking error coefficients. The VCII tracking errors may result in slight changes in the gain values of the realized inversed filters. Nevertheless, the pre-distortion values of R_A, R_B, C_A, or C_B can compensate for this impact without affecting the ω_0 value.

Table 6. Non-ideal parameters of the first-order VM inverse filter in Figure 2a.

Filter type	Transfer function, $G_{v1}(s)=\frac{V_{out1}(s)}{V_{in}(s)}$	Minimum gain (G_0)	Cut-off frequency (ω_0)
ILP	$G_0(sR_1C_1+1)$	$\frac{\alpha_1\beta_1C_A}{C_1}$	$\frac{1}{R_1C_1}$
IHP	$G_0\left(\frac{sR_1C_1+1}{sR_1C_1}\right)$	$\frac{\alpha_1\beta_1R_1}{R_A}$	

Table 7. Non-ideal parameters of the second-order VM inverse filter in Figure 2b.

Filter type	Transfer function, $G_{v2}(s)=\frac{V_{out2}(s)}{V_{in}(s)}$	Minimum gain (G_0)	Cut-off frequency (ω_0)	Quality factor (Q)
ILP	$G_0N(s)$	$\frac{\alpha_1\alpha_2\beta_1\beta_2C_AC_B}{C_1C_2}$	$\frac{1}{\sqrt{R_1R_2C_1C_2}}$	$\frac{\sqrt{R_1R_2C_1C_2}}{R_1C_1+R_2C_2}$
IHP	$G_0\left[\frac{N(s)}{s^2R_1R_2C_1C_2}\right]$	$\frac{\alpha_1\alpha_2\beta_1\beta_2R_1R_2}{R_AR_B}$		
IBP	$G_0\left[\frac{N(s)}{s(R_1C_1+R_2C_2)}\right]$	$(\alpha_1\alpha_2\beta_1\beta_2)\left(\frac{R_1}{C_2}+\frac{R_2}{C_1}\right)\left(\frac{C_A}{R_B}\right)$		

Table 8. Non-ideal parameters of the first-order CM inverse filter in Figure 3a.

Filter type	Transfer function, $G_{i1}(s)=\frac{I_{out1}(s)}{I_{in}(s)}$	Minimum gain (G_0)	Cut-off frequency (ω_0)
ILP	$G_0(sR_1C_1+1)$	$\frac{\alpha_1\beta_1\beta_2C_A}{C_1}$	$\frac{1}{R_1C_1}$
IHP	$G_0\left(\frac{sR_1C_1+1}{sR_1C_1}\right)$	$\frac{\alpha_1\beta_1\beta_2R_1}{R_A}$	

Table 9. Non-ideal parameters of the second-order CM inverse filter in Figure 3b.

Filter type	Transfer function, $G_{i2}(s)=\frac{I_{out2}(s)}{I_{in}(s)}$	Minimum gain (G_0)	Cut-off frequency (ω_0)	Quality factor (Q)
ILP	$G_0N(s)$	$\frac{\alpha_1\alpha_2\beta_1\beta_2\beta_3C_AC_B}{C_1C_2}$	$\frac{1}{\sqrt{R_1R_2C_1C_2}}$	$\frac{\sqrt{R_1R_2C_1C_2}}{R_1C_1+R_2C_2}$

IHP	$G_0\left[\dfrac{N(s)}{s^2R_1R_2C_1C_2}\right]$	$\dfrac{\alpha_1\alpha_2\beta_1\beta_2\beta_3R_1R_2}{R_AR_B}$
IBP	$G_0\left[\dfrac{N(s)}{s\left(R_1C_1+R_2C_2\right)}\right]$	$\left(\alpha_1\alpha_2\beta_1\beta_2\beta_3\right)\left(\dfrac{R_1}{C_2}+\dfrac{R_2}{C_1}\right)\left(\dfrac{C_A}{R_B}\right)$

6. Parasitic Element Analysis

To conduct a further non-ideality analysis, it is necessary to consider the effect of the VCII parasitics on the filter characteristics. For this purpose, we use the non-ideal behavior model of the VCII, which includes a finite non-zero input resistance R_y at port y, a parasitic resistance R_x in parallel with a parasitic capacitance C_x at port x, and a low z-port resistance R_z. Figure 4 illustrates the equivalent circuit for the non-ideal VCII with its parasitic elements.

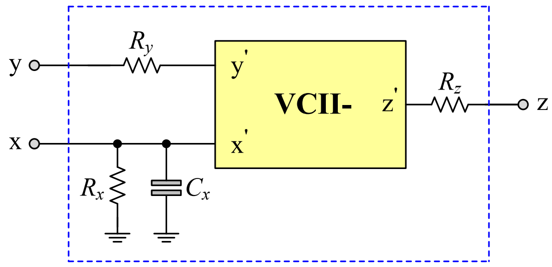

Figure 4. Non-ideal equivalent circuit for the VCII with its parasitics.

6.1. Parasitic Effects on VM Inverse Filter Realization

A straightforward analysis of the proposed first-order VM inverse filter in Figure 2a using the VCII's non-ideal model in Figure 4 yields the non-ideal transfer functions of the ILP and IHP filters given by the following expressions:

1st-order ILP: $$G_{v1}(s)=\frac{G_0\left(sR_1C_1+1\right)}{\left(sR_1C_x+1\right)\left(sR_yC_A+1\right)}\ , \tag{7}$$

1st-order IHP: $$G_{v1}(s)=\frac{G_0\left(sR_1C_1+1\right)}{\left(sR_1C_1\right)\left(sR_1C_x+1\right)}\ . \tag{8}$$

Typically, the value of R_x is extremely high, while the values of R_y and C_x are extremely small. As a consequence, $R_x >> R_1$, $R_A >> R_y$, and $C_x << C_1$. Equations (7) and (8) demonstrate that the VCII parasitics introduce extra poles at frequencies f_{v1} = $(1/2\pi R_1C_x)$ and f_{v2} = $(1/2\pi R_yC_A)$ for ILP filter response, and at frequency f_{v1} in IHP. Therefore, the useful frequencies of the first-order VM ILP and IHP filters are approximated as:

1st-order ILP: $f << \min\ [f_{v1}, f_{v2}]$, (9)

1st-order IHP: $f << \min\ [f_{v1}]$. (10)

For instance, if the parasitic elements of the VCII- are R_y = 38.88 Ω, R_x = 109.24 kΩ, R_z = 38.23 Ω, and C_x = 3 pF [32], and the filter components are chosen as: R_1 = 1 kΩ and C_A = 100 pF, then the pole frequencies will be located at frequencies f_{v1} = 53.08 MHz and f_{v2} = 40.93 MHz. This implies that the first-order VM ILP and IHP filters proposed here have high frequency limitations of approximately 40.93 MHz and 53.05 MHz, respectively.

By taking into account the VCII parasitic effect on the second-order VM inverse filter realization of Figure 2b, the non-ideal transfer functions of ILP, IHP, and IBP filters are as follows:

2nd-order ILP: $$G_{v2}(s)=\frac{G_0N(s)}{\left(sR_1C_{x1}+1\right)\left(sR_2C_{x2}+1\right)\left(sR_{y1}C_A+1\right)\left(sR_{y2}C_B+1\right)},\tag{11}$$

2nd-order IHP: $$G_{v2}(s)=\frac{G_0N(s)}{\left(s^2R_1R_2C_1C_2\right)\left(sR_1C_{x1}+1\right)\left(sR_2C_{x2}+1\right)},\tag{12}$$

2nd-order IBP: $$G_{v2}(s)=\frac{G_0N(s)}{s\left(R_1C_1+R_2C_2\right)\left(sR_1C_{x1}+1\right)\left(sR_2C_{x2}+1\right)\left(sR_{y1}C_A+1\right)},\tag{13}$$

where C_{xk} and R_{yk} are the parasitic elements C_x and R_y of the k-th VCII-. Suppose that $f'_{v1}=\frac{1}{2\pi R_1C_{x1}}$, $f''_{v1}=\frac{1}{2\pi R_2C_{x2}}$, $f'_{v2}=\frac{1}{2\pi R_{y1}C_A}$, and $f''_{v1}=\frac{1}{2\pi R_{y2}C_B}$, then the operating frequency ranges of the proposed second-order VM ILP, IHP, and IBP filters can be defined as:

2nd-order ILP: $$f \ll \min\left[f'_{v1}, f''_{v1}, f'_{v2}, f''_{v2}\right],\tag{14}$$

2nd-order IHP: $$f \ll \min\left[f'_{v1}, f''_{v1}\right],\tag{15}$$

2nd-order IBP: $$f \ll \min\left[f'_{v1}, f''_{v1}, f'_{v2}\right].\tag{16}$$

These effects on the realized filter performance can be considerably minimized if the operating frequencies are chosen sufficiently lower than the parasitic pole frequencies of VCII-.

6.2. Parasitic Effects on CM Inverse Filter Realization

The non-ideal transfer functions of the proposed CM first-order inverse filter in Figure 3a are derived by accounting for the parasitic nature of the VCII-:

1st-order ILP: $$G_{i1}(s)=\frac{G_0\left(sR_1C_1+1\right)}{\left(sR_1C_{x1}+1\right)\left[s\left(R_{z1}+R_{y2}\right)C_A\right]},\tag{17}$$

1st-order IHP: $$G_{i1}(s)=\frac{G_0\left(sR_1C_1+1\right)}{\left(sR_1C_1\right)\left(sR_1C_{x1}+1\right)}.\tag{18}$$

Let $f_{i1}=\frac{1}{2\pi R_1C_{x1}}$ and $f_{i2}=\frac{1}{2\pi\left(R_{z1}+R_{y2}\right)C_A}$, then the frequency limitations of the proposed first-order CM ILP and IHP filters should be lied in the following ranges:

1st-order ILP: $$f \ll \min\left[f_{i1}, f_{i2}\right],\tag{19}$$

1st-order IHP: $$f \ll \min\left[f_{i1}\right].\tag{20}$$

Furthermore, we have also considered the parasitic effect on the proposed CM second-order inverse filter structure in Figure 3b. The various non-ideal expressions of ILP, IHP, and IBP filter responses are given by:

2nd-order ILP:

$$G_{i2}(s)=\frac{G_0N(s)}{\left(sR_1C_{x1}+1\right)\left(sR_2C_{x2}+1\right)\left[s\left(R_{z1}+R_{y2}\right)C_A+1\right]\left[s\left(R_{z2}+R_{y3}\right)C_B+1\right]},\tag{21}$$

 doi:10.20944/preprints202501.0957.v1

2nd-order IHP:

$$G_{i2}(s) = \frac{G_0 N(s)}{s^2 R_1 R_2 C_1 C_2 \left(sR_1 C_{x1} + 1\right)\left(sR_2 C_{x2} + 1\right)}, \tag{22}$$

2nd-order IBP:

$$G_{i2}(s) = \frac{G_0 N(s)}{s\left(R_1 C_1 + R_2 C_2\right)\left(sR_1 C_{x1} + 1\right)\left(sR_2 C_{x2} + 1\right)\left[s\left(R_{z1} + R_{y2}\right)C_A + 1\right]}, \tag{23}$$

which represent the additional pole frequencies expressed by: $f'_{i1} = \frac{1}{2\pi R_1 C_{x1}}$, $f''_{i1} = \frac{1}{2\pi R_2 C_{x2}}$, $f'_{i2} = \frac{1}{2\pi\left(R_{z1} + R_{y2}\right)C_A}$, and $f''_{i2} = \frac{1}{2\pi\left(R_{z2} + R_{y3}\right)C_B}$.

Therefore, the frequency ranges of operation of the proposed CM second-order inverse filter in Figure 3b can be approximated from the above relations as:

2nd-order ILP: $f \ll \min\,[\,f'_{i1}, f''_{i1}, f'_{i2}, f''_{i2}\,]$, (24)

2nd-order IHP: $f \ll \min\,[\,f'_{i1}, f''_{i1}\,]$, (25)

2nd-order IBP: $f \ll \min\,[\,f'_{i1}, f''_{i1}, f'_{i2}\,]$. (26)

7. Simulation Verification of Filter Responses

The validity of the cascadable inverse filters proposed in Figures 2 and 3 has been evaluated through a simulation conducted by PSPICE program. In the simulation analysis, the CMOS structure of the VCII- as shown in Figure 5 has been implemented [33]-[34]. The ratio of width (W) to channel length (L) of the CMOS transistors employed is listed in Table 10. Supply voltages of +V = -V = 0.75 V and biasing currents of $I_{B1} = I_{B2} = 25$ µA are used. All the proposed inverse filter structures are tested with identical resistors and capacitors: $R_1 = R_2 = R_A = R_B = 1$ kΩ, and $C_1 = C_2 = C_A = C_B = 100$ pF for the theoretical pole frequency of $f_0 = \omega_0/2\pi = 1.59$ MHz.

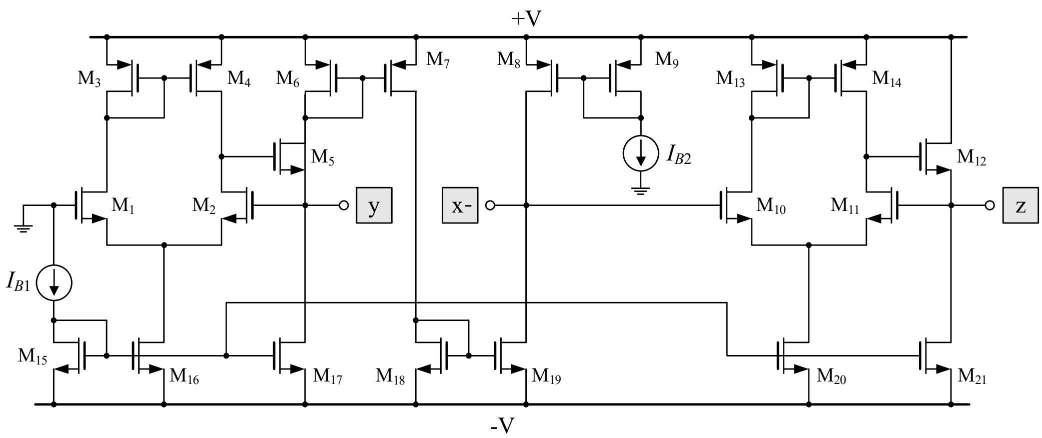

Figure 5. CMOS implementation of VCII-.

The simulated time and frequency responses of the VM and CM inverse filters in Figures 2 and 3 compared with the theoretical responses are given in Figures 6-9. The proposed circuits are tested at a signal frequency of 1.59 MHz with an input signal amplitude of 50 mV (peak) for VM and 50 µA (peak) for CM. The total power consumptions of the first- and second-order VM inverse filters are 0.255 mW and 0.511 mW, respectively, while the first- and second-order CM inverse filters are 0.511 mW and 0.766 mW.

Preprints.org (www.preprints.org) | NOT PEER-REVIEWED | Posted: 14 January 2025 doi:10.20944/preprints202501.0957.v1

The simulated cut-off frequency f_0 for the first-order VM ILP and IHP responses was measured at 1.56 MHz and 1.54 MHz, respectively, and the corresponding f_0 values for the second-order ILP, IHP, and IBP responses were 1.57 MHz, 1.52 MHz, and 1.55 MHz. For the CM inverse filters, the simulated f_0 values of the first-order ILP and IHP responses were 1.57 MHz and 1.50 MHz, while the second-order ILP, IHP, and IBP filters provided the simulated f_0 at 1.57 MHz, 1.52 MHz, and 1.56 MHz, respectively.

Table 10. W/L of the MOS transistors in Figure 5.

Transistors	W/L (μm/μm)
M_1 - M_2, M_{10} - M_{11}	10/0.18
M_3 - M_4, M_6 - M_7, M_8 - M_9, M_{13} - M_{14}	5/0.18
M_5, M_{12}	50/0.18
M_{15} - M_{21}	3/0.18

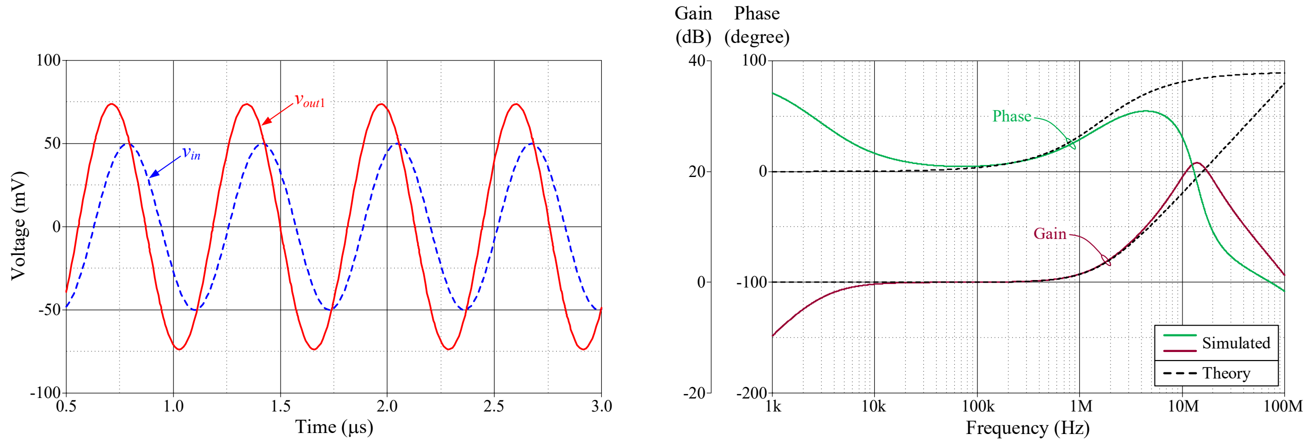

(a)

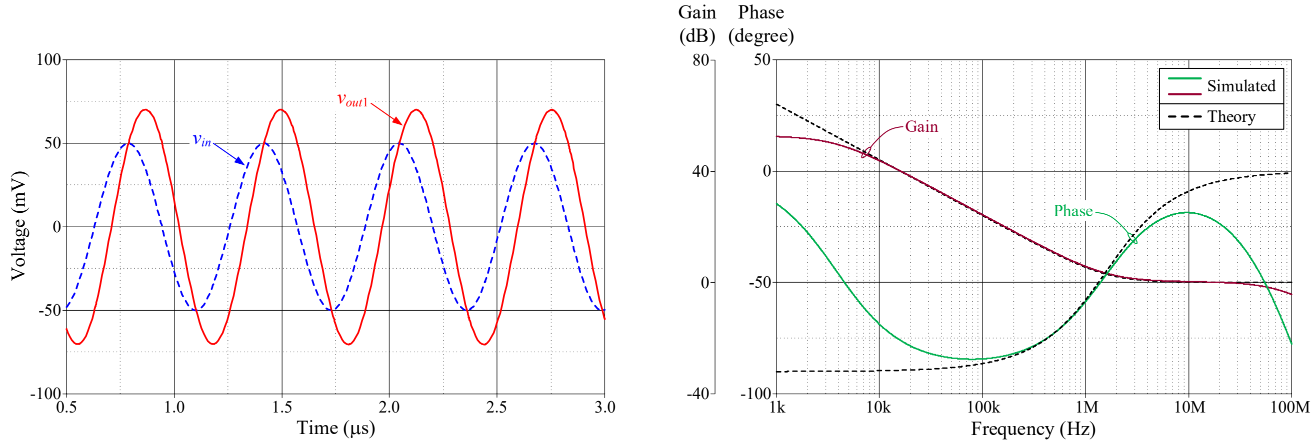

(b)

Figure 6. Time and frequency responses of the first-order VM inverse filter in Figure 2a. (**a**) ILP responses; (**b**) IHP responses.

Preprints.org (www.preprints.org) | NOT PEER-REVIEWED | Posted: 14 January 2025 doi:10.20944/preprints202501.0957.v1

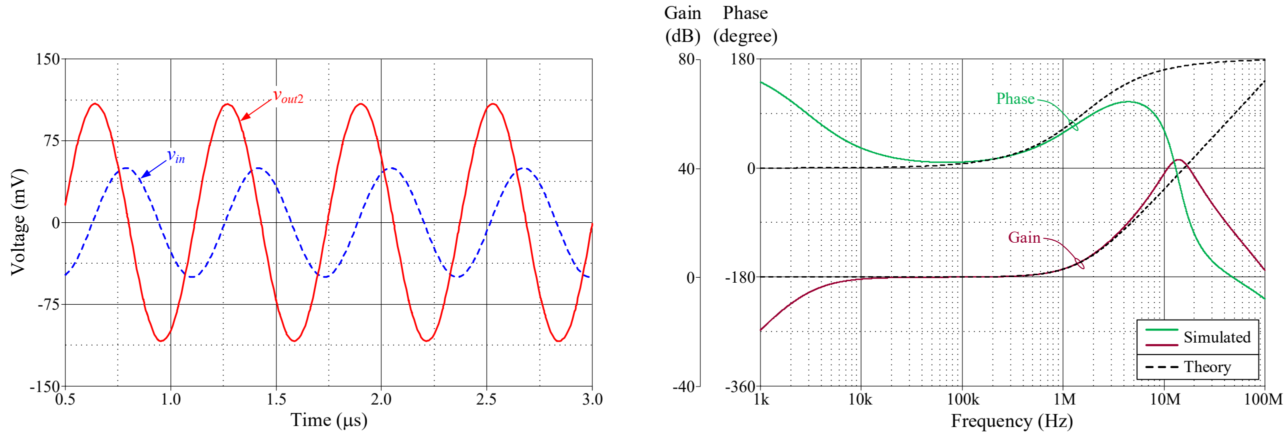

(a)

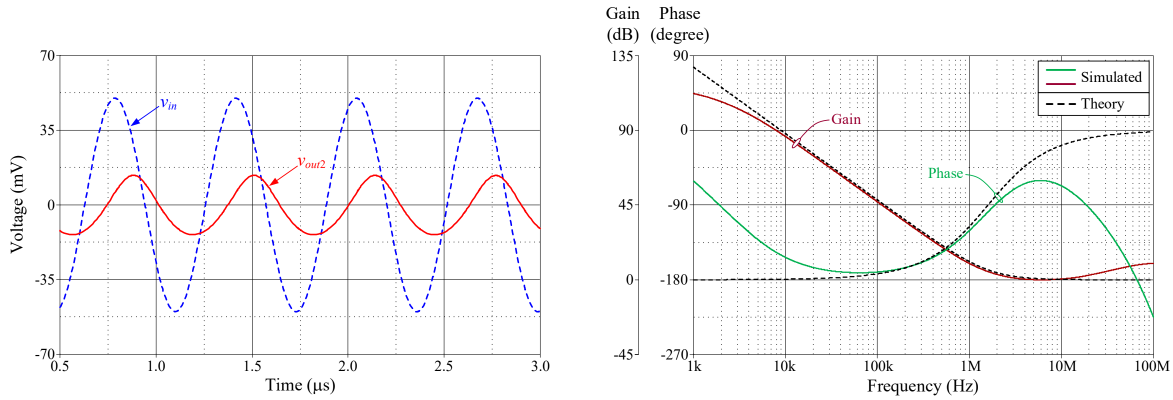

(b)

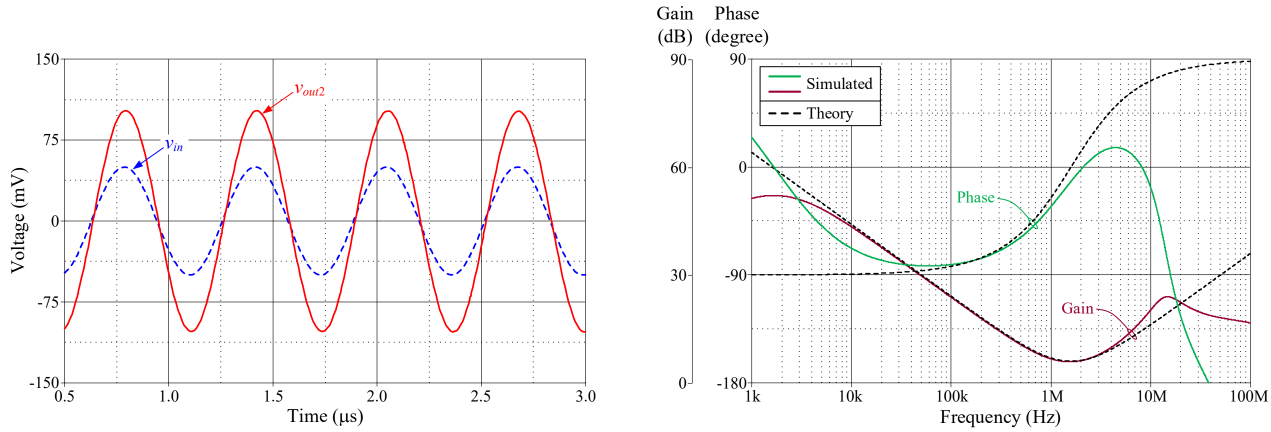

(c)

Figure 7. Time and frequency responses of the second-order VM inverse filter in Figure 2b. (**a**) ILP responses; (**b**) IHP responses; (c) IBP responses.

Preprints.org (www.preprints.org) | NOT PEER-REVIEWED | Posted: 14 January 2025 doi:10.20944/preprints202501.0957.v1

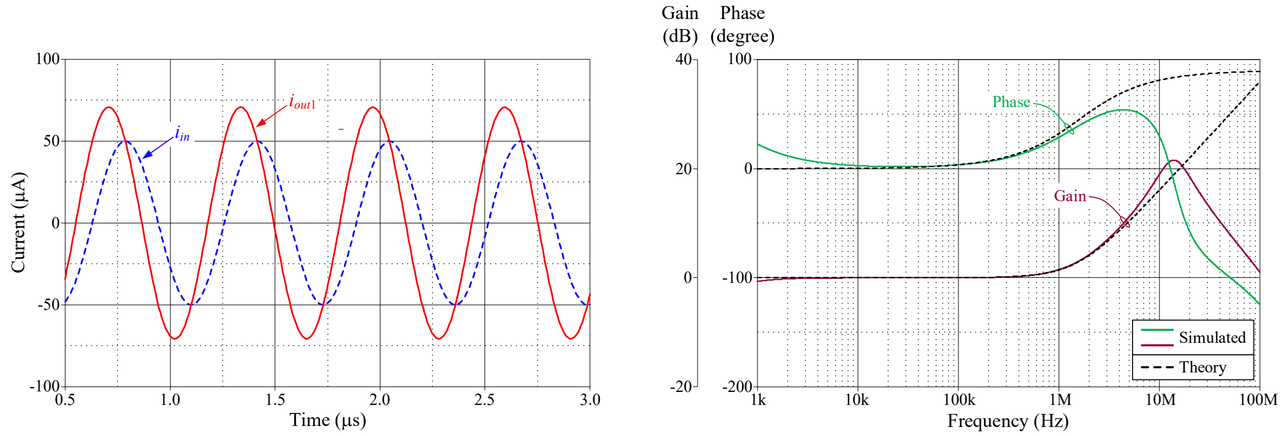

(a)

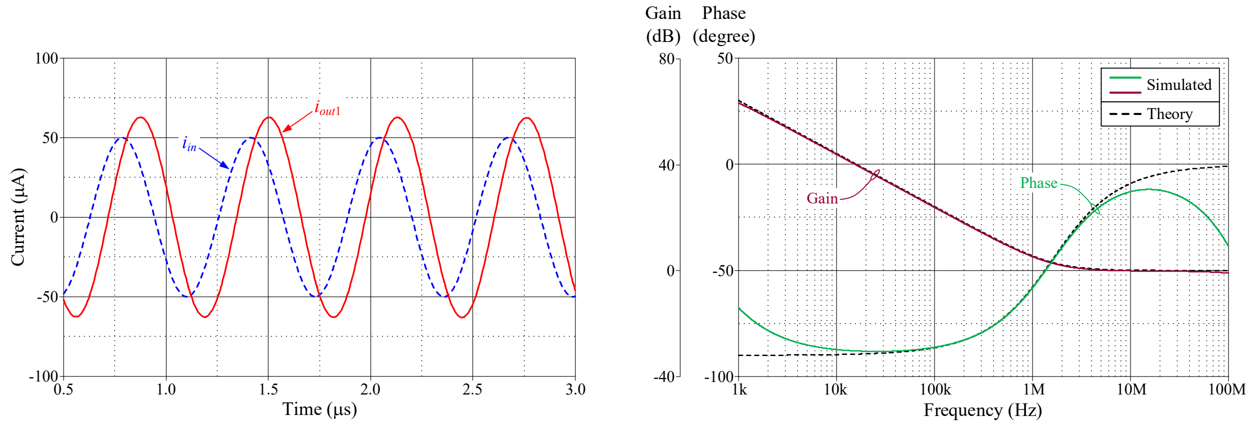

(b)

Figure 8. Time and frequency responses of the first-order CM inverse filter in Figure 3a. (**a**) ILP responses; (**b**) IHP responses.

The f_o-tuning for the IBP filter in Figure 2b was simulated with a constant value of Q. The capacitor and resistor values are $C_1 = C_2 = C_A = 100$ pF, $R_B = 1$ kΩ, and $R_1 = R_2 = 0.5$ kΩ, 2 kΩ, and 5 kΩ. With a fixed Q-value of 0.5, the corresponding values for f_0 are 3.18 MHz, 795.77 MHz, and 318.31 MHz, respectively. Figure 10 illustrates the ideal and simulated gain-frequency responses, demonstrating the ability to independently adjust the f_0-value of the proposed filter. The proposed VM IBP filter in Figure 2b was also simulated at different temperatures including 0˚C, 25˚C, 50˚C, 75˚C, and 100˚C. The simulations were conducted with $C_1 = C_2 = C_A = 100$ pF and $R_1 = R_2 = R_B = 1$ kΩ, and the obtained results are shown in Figure 11. At $f_0 = 1.59$ MHz, the deviations from its nominal value in voltage gain due to temperature variations are approximately -0.88 dBV at 0˚C and +7.10 dBV at 100˚C, which can be considered insignificant.

Preprints.org (www.preprints.org) | NOT PEER-REVIEWED | Posted: 14 January 2025 doi:10.20944/preprints202501.0957.v1

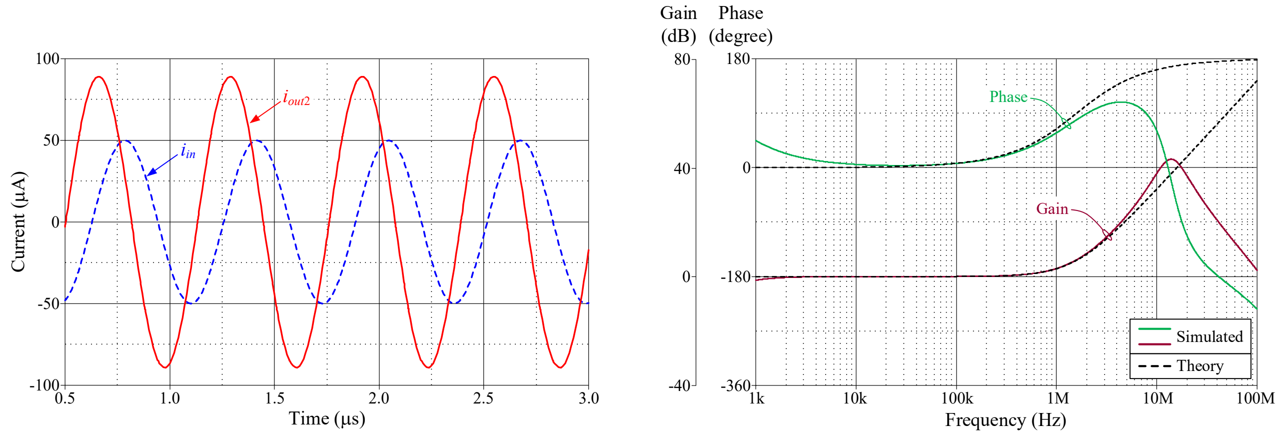

(a)

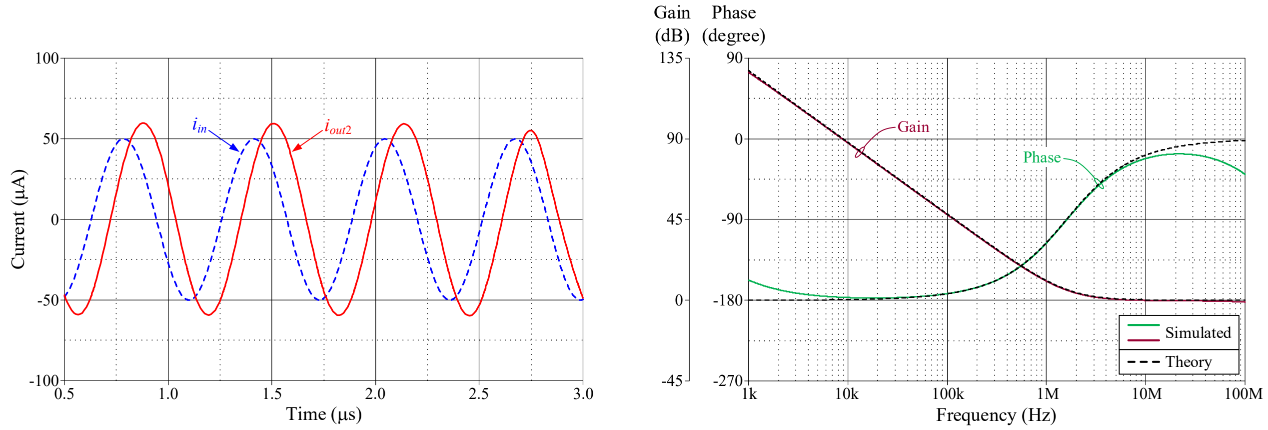

(b)

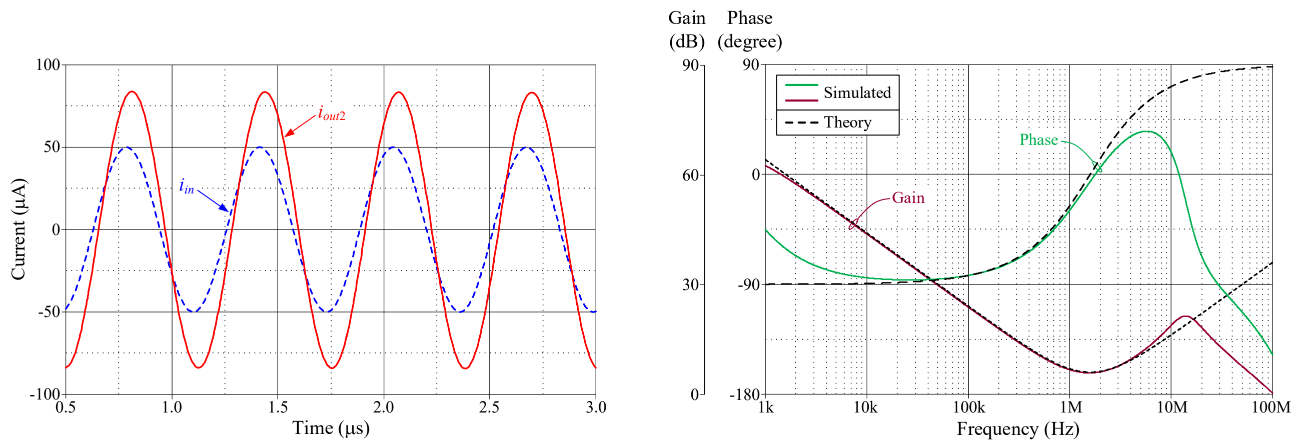

(c)

Figure 9. Time and frequency responses of the second-order CM inverse filter in Figure 3b. (**a**) ILP responses; (**b**) IHP responses; (c) IBP responses.

Preprints.org (www.preprints.org) | NOT PEER-REVIEWED | Posted: 14 January 2025 doi:10.20944/preprints202501.0957.v1

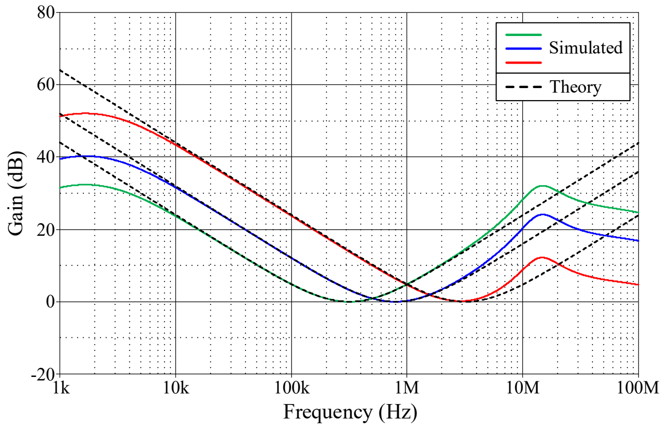

Figure 10. f_o-tuning responses of the IBP filter circuit in Figure 2b for constant Q value.

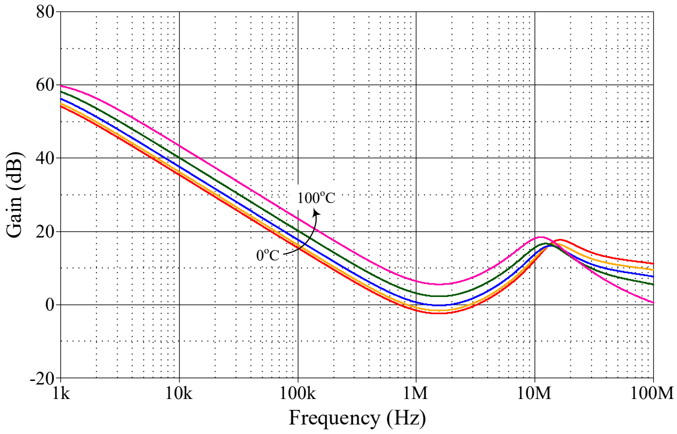

Figure 11. Frequency responses of the IBP filter circuit in Figure 2b at different temperatures (0˚C, 25˚C, 50˚C, 75˚C, and 100˚C).

Furthermore, a Monte Carlo (MC) statistical analysis was performed on the VM IBP filter at the pole frequency of 1.59 MHz, considering nominal 5% tolerances in the values of resistors and capacitors. Figure 12 depicts the MC simulation results with a Gaussian distribution for 200 runs. The standard deviation in f_o resulting from the changes in resistor and capacitor tolerances was obtained at 47.92 kHz, even though it is not considerable.

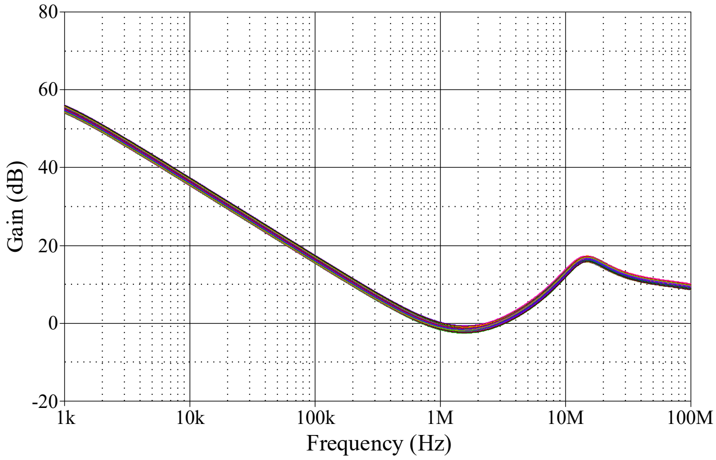

Figure 12. Monte Carlo statistical analysis results of the VM IBP filter response.

8. Experimental Verification

The experimental laboratory measurement has been carried out to further validate the practicability of the proposed design. For this purpose, the practical VCII- has been realized using commercially available IC-type AD844s, as shown in Figure 13 [34]. The DC bias voltages were set to +V = -V = 5 V. The resistor and capacitor have values of R_1 = 1 kΩ and C_1 = C_A = 1 nF, respectively, to obtain an ideal pole frequency of f_o = 159 kHz. Figure 14 shows the experimentally measured time and frequency responses for the proposed first-order VM inverse filter in Figure 2a along with the corresponding ideal responses. The input voltage was set at 100 mV peak-to-peak with a frequency of 159 kHz. The testing results, thus, verify the feasibility of the proposed concept.

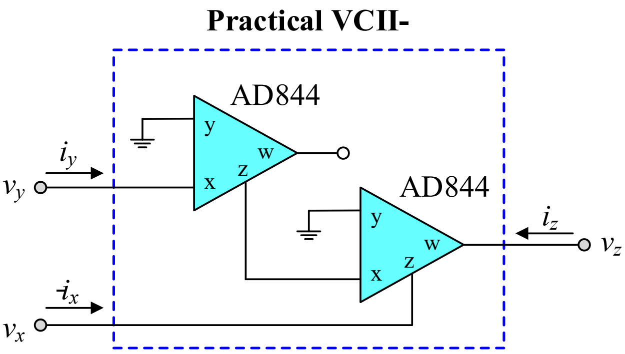

Figure 13. Practical realization of the VCII- using commercially available IC AD844s.

9. Conclusions

Four circuit configurations for realizing first- and second-order inverse filters using second-generation voltage conveyors (VCIIs) have been presented in this paper. Both proposed first-order inverse filters in VM and CM can realize inverse LP and HP filter functions using the same circuit topology by the appropriate selection of the branch impedance. Using the same circuit concept, both of the proposed second-order VM and CM inverse filters can provide inverse LP, BP, and HP filter functions from a single design. All the suggested circuits are appropriate for cascade connections. By modifying the passive element values, it is possible to independently control the pole frequency and gain of the filters. Analyses of non-ideal performance, such as transfer errors and parasitic effects, have been examined in relation to theoretical performance. The feasibility of the circuits was confirmed by PSPICE simulations in conjunction with laboratory testing measurements.

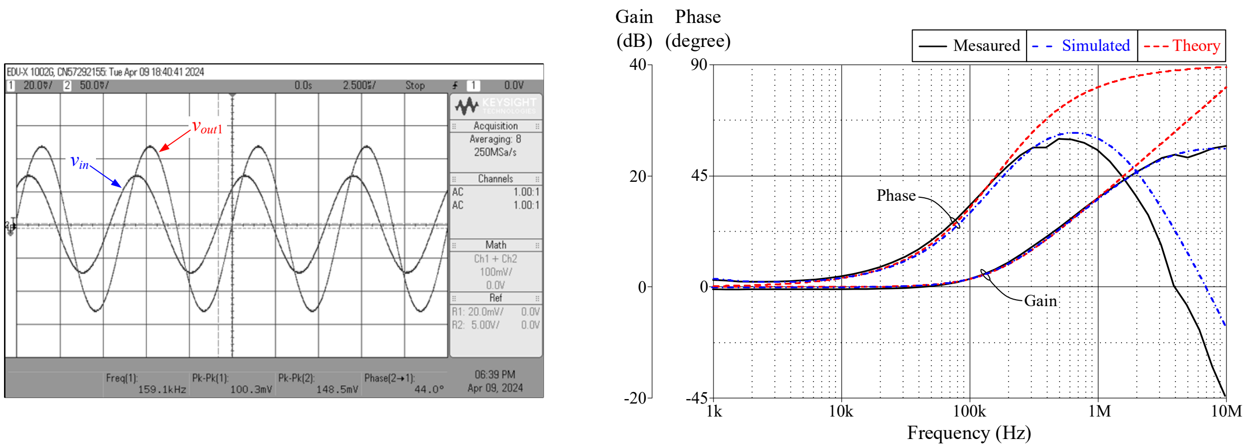

(a)

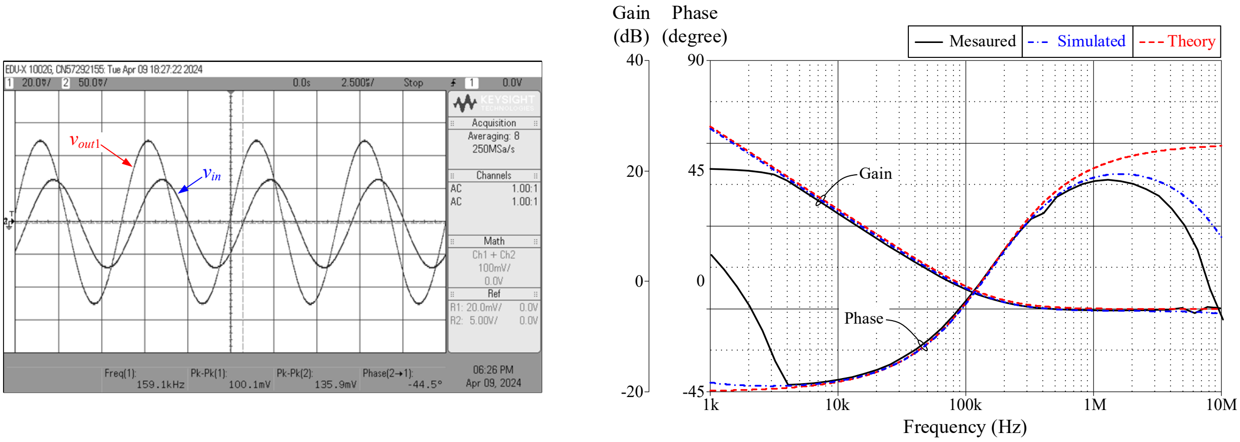

(b)

Figure 14. Experimentally measured time and frequency responses for the first-order VM inverse filter in Figure 2a. (**a**) ILP responses; (**b**) IHP responses.

Author Contributions: Conceptualization, N.R. and W.T.; methodology, N.R. and W.T.; software, N.R. and N.L.; validation, N.R., N.L., T.P., M.F, and W.T.; formal analysis, T.P., M.F. and W.T.; investigation, N.R., T.P., and W.T.; resources, N.R. and N.L.; data curation, T.P., and M.F.; writing—original draft preparation, N.R. and N.L.; writing—review and editing, T.P., M.F, and W.T; visualization, N.R., T.P., and W.T.; supervision, T.P., M.F, and W.T; project administration, N.L.; funding acquisition, N.L., W.T. All authors have read and agreed to the published version of the manuscript.

Funding: This work was financially supported by King Mongkut's Institute of Technology Ladkrabang [2568-02-01-001].

Institutional Review Board Statement: Not applicable.

Informed Consent Statement: Not applicable.

Acknowledgments: The authors appreciate the support and infrastructure provided by the Department of Instrumentation and Control Engineering, School of Engineering, King Mongkut's Institute of Technology Ladkrabang for the completion of this work.

Conflicts of Interest: The authors declare no conflicts of interest.

Abbreviations

The following abbreviations are used in this manuscript:

R	Resistor
C	Capacitor
N/A	Not available
OA	Operational Amplifier
FTFN	Four Terminal Floating Nullor
CCII	Second-Generation Current Conveyor
CDTA	Current Differencing Transconductance Amplifier
CFOA	Current Feedback Operational Amplifier
MCFOA	Modified Current Feedback Operational Amplifier
CDBA	Current Differencing Buffered Amplifier
OTA	Operational Transconductance Amplifier
OTRA	Operational Transresistance Amplifier
VDTA	Voltage Differencing Transconductance Amplifier
VCVS	Voltage-Controlled Voltage Source
SW	Analog switch

References

1. Leuciuc, A. Using nullors for realisation of inverse transfer functions and characteristics. *Electron. Lett.* **1997**, *33*, 949–951.
2. Chipipop, B.; Surakampontorn, W. Realisation of current-mode FTFN-based inverse filter. *Electron. Lett.* **1999**, *35*, 690–692.
3. Wang, H. Y.; Lee, C. T. Using nullors for realisation of current-mode FTFN-based inverse filters. *Electron. Lett*. **1999**, *35*, 1889–1890.
4. Abuelma'atti, M. T. Identification of cascadable current-mode filters and inverse-filters using single FTFN. *Frequenz* **2000**, *54*, 1889–289.
5. Shah, N. A.; Malik, M. A. FTFN-based dual inputs current-mode allpass inverse filters. *Indian J. Radio Space Phys.* **2005**, *34*, 206–209.
6. Shah, N. A.; Rather, M. F. Realization of voltage-mode CCII-based allpass filter and its inverse version. *Indian J. Pure Appl. Phys.* **2006**, *44*, 269–271.
7. Shah, N. A.; Quadri, M.; Iqbal, S. Z. High output impedance current-mode allpass inverse filter using CDTA. *Indian J. Pure Appl. Phys*. **2008**, *44*, 893–896.
8. Gupta, S. S.; Bhaskar, D. R.; Senani, R.; Singh, A. K.; Inverse active filters employing CFOAs. *Electr. Eng.* **2009**, *91*, 23–26.
9. Wang, H. Y.; Chang, S. H.; Yang, T. Y.; Tsai, P. Y. A novel multifunction CFOA-based inverse filter. *Circuits Syst*. **2011**, *2*, 14–17.
10. Gupta, S. S.; Bhaskar, D. R.; Senani, R. New analogue inverse filters realised with current feedback op-amps. *Int. J. Electron*. **2011**, *98*, 1103–1113.
11. Garg, K.; Bhagat, R.; Jaint, B. A novel multifunction modified CFOA based inverse filter. *In Proc.* ***2012 IEEE 5th Indian Int. Conf. Power Electronics (IICPE)*****, 6-8 Dec. 2012.**
12. Nasir, A. R.; Ahmad, S. N. A new current-mode multifunction inverse filter using CDBAs. *Int. J. Comput. Sci. Infor. Sec*. **2013**, *11*, 50–52.
13. Pandey, R.; Pandey, N.; Negi, T.; Garg, V. CDBA based universal inverse filter. ISRN Electronics **2013**, *2013*, Article ID 181869, 6 pages.
14. Tsukutani, T.; Sumi, Y.; Yabuki, N. Electronically tunable inverse active filters employing OTAs and grounded capacitors. *Int. J. Electron. Lett*. **2014**, *4*, 1–11.
15. Patil, V.; Sharma, R. K. Novel inverse active filters employing CFOAs. *Int. J. for Sci. Research & Development*, **2015**, *3*, 359–360.
16. Sharma, A.; Kumar, A.; Whig, P. On the performance of CDTA based novel analog inverse low pass filter using 0.35 µm CMOS parameter. *Int. J. Sci. Tech. Manage*. **2015**, *4*, 594–601.
17. Tsukutani, T.; Kunugasa, Y.; Yabuki, N. CCII-based inverse active filters with grounded passive components. *J. Electr. Eng*. **2018**, *6*, 212-215.
18. Singh, A. K.; Gupta, A.; Senani, R. OTRA-based multi-function inverse filter configuration. *Advances Electr. Electron. Eng*. **2017**, *15*, 846–856.
19. Kumar, P.; Pandey, N.; Paul, S. K. Realization of resistorless and electronically tunable inverse filters using VDTA. *J. Circuits Syst. Comput*. **2019**, *28*, 1950143, 20 pages.
20. Pradhan, A.; Sharma, R. K. Generation of OTRA-based inverse all pass and inverse band reject filters. *Proc. Natl. Acad. Sci., India, Sect. A Phys. Sci*. **2020**, *90*, 481–491.
21. Bhagat, R.; Bhaskar, D. R.; Kumar, P. Inverse band reject and all pass filter structure employing CMOS CDBAs. *Int. J. Eng. Research Tech*. **2019**, *8*, 39–44.
22. Bhagat, R.; Bhaskar, D. R.; Kumar, P. Multifunction filter/inverse filter configuration employing CMOS CDBAs. *Int. J. Recent Tech. Eng*. **2019**, *8*, 8844–8853.
23. Kamat, D. V. New operational amplifier based inverse filters. *In Proc. Third Int. Conf. Electron. Commun. Aerospace Tech*. Coimbatore, India, June 12-14, 2019; pp. 1177-1181.
24. Banerjee, S.; Borah, S. S.; Ghosh, M.; Mondal, P. Three novel configurations of second order inverse band reject filter using a single operational transresistance amplifier. *In Proc. 2019 IEEE Region 10 Conference (TENCON 2019*), Oct. 17-20, 2019, Kerala, India; pp. 2173-2178.

25. Borah, S. S.; Singh, A.; Ghosh, M. CMOS CDBA based 6th order inverse filter realization for low-power applications. *In Proc. 2020 IEEE Region 10 Conference (TENCON 2020)*, Nov. 16-19, 2020, Osaka, Japan; pp. 11-16.
26. Kumar, P.; Pandey, N.; Paul, S. K.; Electronically tunable VDTA-based multi-function inverse filter. *Iran. J. Sci. Technol. - Trans. Electr. Eng.* **2021**, *45*, 247–257.
27. Raj, A.; Bhagat, R.; Kumar, P.; Bhaskar, D. R. Grounded-capacitor analog inverse active filters using CMOS OTAs. *In Proc. 2021 8th Int. Conf. Signal Process. Integrated Networks (SPIN*), Aug. 26-27, 2021, Noida, India; pp. 778-783.
28. Paul, T. K.; Roy, S.; Pal, R. R. Realization of inverse active filters using single current differencing buffered amplifier. *J. Sci. Research*, **2021**, *13*, 85-99.
29. Al-Absi, M. A. Realization of inverse filters using second generation voltage conveyor (VCII). *Analog Integr. Circuits Signal Process*. **2021**, *109*, 29–32.
30. Al-Shahrani, S. M.; Al-Absi, M. A. Efficient inverse filters based on second-generation voltage conveyor (VCII). *Arabian J. Sci. Eng*. **2022**, *47*, 2685–2690.
31. Nako, J.; Psychalinos, C.; Minaei, S. Single-input multiple-output inverse filters designs with cascade capability. Int. J. Electron. Commun. (AEÜ) **2024**, *175*, 155061.
32. Safari, L.; Yuce, E.; Minae, S.; Ferri, G.; Stornelli, V. A second-generation voltage conveyor (VCII)-based simulated, grounded inductor. *Int. J. Circuit Theory Appl*. **2020**, *48*, 1–14.
33. Faseehuddin, M.; Shireen, SAli, .; S. H. M.; Tangsrirat, W. Novel lossless positive/negative grounded capacitance multipliers using VCII. *Elektronika ir Elektrotechnika*, **2023**, *29*, 19-26.
34. Faseehuddin, M.; Shireen, S.; Herencsar, N.; Tangsrirat, W. Novel FDNR, FDNC and lossy inductor simulators employing second generation voltage conveyor (VCII). *Int. J. Numer. Model.: Electronic Networks, Devices and Fields*, **2023**, *36*, 1-15.